LABORATORY INVESTIGATION

Characterization of Irreversible Electroporation Ablation with a Validated Perfused Organ Model

Suyashree Bhonsle, MS, Mohammad Bonakdar, PhD,
Robert E. Neal, II, PhD, Charles Aardema, BS, John L. Robertson, VMD, PhD,
Jonathon Howarth, BS, Helen Kavnoudias, BMedSci, PhD,
Kenneth R. Thomson, MBChB, MD, S. Nahum Goldberg, MD, MSc, and
Rafael V. Davalos, PhD

ABSTRACT

Purpose: To develop and validate a perfused organ model for characterizing ablations for irreversible electroporation (IRE)–based therapies.

Materials and Methods: Eight excised porcine livers were mechanically perfused with a modified phosphate-buffered saline solution to maintain viability during IRE ablation. IRE pulses were delivered using 2 monopolar electrodes over a range of parameters, including voltage (1,875–3,000 V), pulse length (70–100 μsec), number of pulses (50–600), electrode exposure (1.0–2.0 cm), and electrode spacing (1.5–2.0 cm). Organs were dissected, and treatment zones were stained with triphenyl tetrazolium chloride to demonstrate viability and highlight the area of ablation. Results were compared with 17 in vivo ablations performed in canine livers and 35 previously published ablations performed in porcine livers.

Results: Ablation dimensions in the perfused model correlated well with corresponding in vivo ablations ($R^2 = 0.9098$) with a 95% confidence interval of < 2.2 mm. Additionally, the validated perfused model showed that the IRE ablation zone grew logarithmically with increasing pulse numbers, showing small difference in ablation size over 200–600 pulses (3.2 mm ± 3.8 width and 5.2 mm ± 3.9 height).

Conclusions: The perfused organ model provides an alternative to animal trials for investigation of IRE treatments. It may have an important role in the future development of new devices, algorithms, and techniques for this therapy.

ABBREVIATIONS

IRE = irreversible electroporation, TTC = triphenyl tetrazolium chloride

Irreversible electroporation (IRE) is a focal ablation therapy that uses high-amplitude, short-duration, pulsed electric fields to induce cell death via the disruption of cell membranes and loss of cell homeostasis (1–4). During IRE treatment, microsecond pulses are delivered using needle electrodes (5), producing localized electric

Appendix A, Figures E1–E3, and Table E1 are available online at www.jvir.org.

field distribution in the target and surrounding tissue. For a given set of pulse parameters and tissue type, cells exposed to electric fields beyond a lethal threshold degenerate. Treatment success depends on accurate prediction of the ablation size for a given parameter set. This can be achieved by the use of treatment-planning algorithms that calculate the induced electric field distribution in the target and surrounding tissue and predict ablation size from a priori knowledge of response of a specific tissue to IRE, including the electric field thresholds of cell death (6,7) and changes in bulk tissue conductivity (8,9).

Commonly, in vitro cell suspensions are used as a model to determine the electric field cell death thresholds (10,11). More recently, three-dimensional tissue mimics have been shown to be superior in predicting the field thresholds in vivo because cell shape in these constructs leads to a more physiologically relevant model (12,13). Nevertheless, both these approaches cannot emulate the change in the bulk conductivity of tissue as observed in vivo, which is necessary for clinical predictability. Although IRE has been rapidly deployed to treat cancer in multiple sites clinically (14–16), substantial opportunity remains to improve understanding of the underlying mechanisms of action for treatment optimization. This requires using models that account for biologic complexities, such as blood perfusion, heterogeneous cell populations, and anisotropy. Insufficiency of in vitro models and the prohibitive expense and time required to conduct in vivo studies have slowed progress of IRE parameter optimization and device investigation.

In this study, results of a hybrid technique developed to circumvent the issues encumbering IRE investigations are reported. Freshly harvested, actively perfused organs combined with viability stains were used to evaluate the ablative characteristics of IRE treatments. Although perfused organ models have been used previously for other thermal ablation techniques (17–19), translating this model to IRE requires a unique approach to attain accurate, predictive outcomes. In contrast to thermal ablation, IRE shows no inherent macroscopic changes in dead tissue, requiring viability stains to visualize ablations, something that is possible only by organ-wide viability. IRE experiments were performed on a perfused organ model of porcine liver using pulse parameters and electrode configurations used in in vivo studies for validated comparison. The goal of the present work was to establish the perfused organ model as a feasible substitute to in vivo experiments (20).

MATERIALS AND METHODS

The efficacy of the perfused organ model was examined for its ability to replicate in vivo outcomes of key system parameters (20), including electrode separation (ie, interelectrode spacing), electrode exposure, applied voltages, and pulse number (**Table 1**). Parameter sets 1–5 (**Table 1**) were chosen to be identical to published IRE experiments on porcine liver (20). The study reported was conducted in one of the author, S.N.G.'s, laboratory, allowing maximum insight into the treatment method. Parameter sets 6–11 were selected based on standard IRE treatment used in clinical applications that resulted in creation of clinically relevant ablation sizes (21,22). Experiments using these parameters were performed on 4 in vivo canine livers in

Table 1. Summary of Treatment Parameters for Perfused Organ Model and Corresponding In Vivo Experiments Performed in This Study or Published Elsewhere

| | | | | | | | | | N | |
Parameter Set	Electrode Separation (cm)	Electrode Exposure (cm)	Pulse Amplitude (V)	V/d	No. Pulses	Pulse Length (μsec)	Delivery Rate (Hz)	Perfused Organ Model	Porcine (30)	Canine
1	1.5	2.0	3,000	2,000	70	70	1	4	9	
2	1.5	2.0	2,650	1,766	70	70	1	4	4	
3	1.5	2.0	2,250	1,500	70	70	1	4	13	
4	1.5	2.0	2,250	1,500	50	70	1	4	5	
5	1.5	2.0	2,250	1,500	90	70	1	4	4	
6	1.5	1.0	1,875	1,250	100	100	1	3		3
7	2.0	1.0	3,000	1,500	100	100	1	21		2
8	1.5	1.0	2,625	1,750	50	100	1	3		3
9	1.5	1.0	2,625	1,750	100	100	1	21		3
10	1.5	1.0	2,625	1,750	200	100	1	3		3
11	1.5	1.0	2,625	1,750	400	100	1	5		3
12	1.5	1.0	2,625	1,750	300	100	1	4		
13	1.5	1.0	2,625	1,750	600	100	1	5		
14	1.5	1.0	2,625	1,750	150	100	1	3		

Note–The electric field from needle electrodes has an inhomogeneous, nonlinear distribution and is highly spatially variable. Therefore, the V/d ratio is provided as a general reference metric for pulse intensity based on needle separation and voltage. V/d = voltage to distance.

addition to the perfused organ model to allow close comparison between the 2 models and to gauge species-to-species differences. Lastly, parameter sets 12–14 were performed on the perfused organ model to gauge the effect of higher pulse numbers on ablation size.

Perfused Organ Model

Organ Preparation. Porcine livers were acquired from a local slaughterhouse/abattoir within 10 minutes of death. Connections were made to the portal vein, hepatic artery, and major hepatic vein using Luer Lock connectors (**Fig E1a, b** [available online at *www.jvir.org*]). Organs were then immediately perfused with modified phosphate-buffered saline (**Appendix A** [available online at *www.jvir.org*]) to flush the vasculature and remove blood clots. Conductivity of the perfusate at room temperature was 1.63 S/m. After flushing, organs were transported on ice to the laboratory, with a total travel time of 120 minutes ± 15.

At the laboratory, the organs were flushed again and connected to the VASOWAVE system (Smart Perfusion -> CAVESWAVE^{TM} system, BioMedInnovations LLC, Denver, North Carolina) for active perfusion (**Fig 1**) (23). Perfusate was delivered at a rate of 60 beats/min with systolic/diastolic perfusion pressure waveforms of 15/5 mm Hg for portal vein and 90/50 mm Hg for hepatic artery and return via the hepatic vein at 0–5 mm Hg. Perfusate temperature was maintained at 11°C using an external chiller to lower the metabolism and preserve the organ for up to 10 hours (24) and enable better matching of electric conductivity to the clinical state (25). Perfusion was paused during each treatment to reduce arcing and resumed between trials. After completion of the IRE treatments (2–3 hours), organs were perfused for an additional 2 hours before harvest to allow sufficient time to observe the treatment effect (26).

Eight livers were used with 8–13 ablations performed per liver. Ablations for which accurate dimensions could not be measured because of traversing blood vessels were discarded. Measurements of 86 ablations were obtained (**Table 1**).

Electroporation Pulse Delivery. After confirmation of sufficient, organ-wide perfusion, observed through uniform inflation of the organ and removal of blood clots, 2 monopolar 19-gauge needle electrodes (AngioDynamics Inc, Latham, New York), including the entire exposed active electrode and 0.5 cm of insulation, were inserted perpendicular to the surface of the liver (**Fig 2a**). IRE treatments were performed using the ECM 830 electroporation pulse generator (BTX Harvard Apparatus, Holliston, Massachusetts). Treatment parameters were selected based on standard IRE treatment used in clinical applications that result in creation of clinically relevant ablation sizes (**Table 1**) (20,27,28).

All pulses were delivered at a rate of 1/s with a pulse width of either 100 μsec or 70 μsec. Three additional parameter sets were performed consisting of 150, 300, and 600 pulses at 2,625 V with an interelectrode separation of 1.5 cm.

Pathologic Analysis. After IRE treatment and 2 hours of additional perfusion, ablation zones were sliced perpendicular to the electrode through the middle plane of the ablation for gross evaluation (**Fig 2a**). To permit more readily definable ablation margins, the largest section in the ablation center was stained with triphenyl tetrazolium chloride (TTC) (MP Biomedicals, LLC, Santa Ana, California) in phosphate-buffered saline (10 gr/L) for 5–10 minutes (28). After staining, ablation height and width were measured (**Fig 2a**). Samples were fixed in formalin overnight, with photographs taken before and after fixation. Ablation sizes were measured before fixation, as fixation can cause some tissue deformation.

Canine Model

In vivo canine liver ablations were performed as approved by an animal ethics committee. Four previously
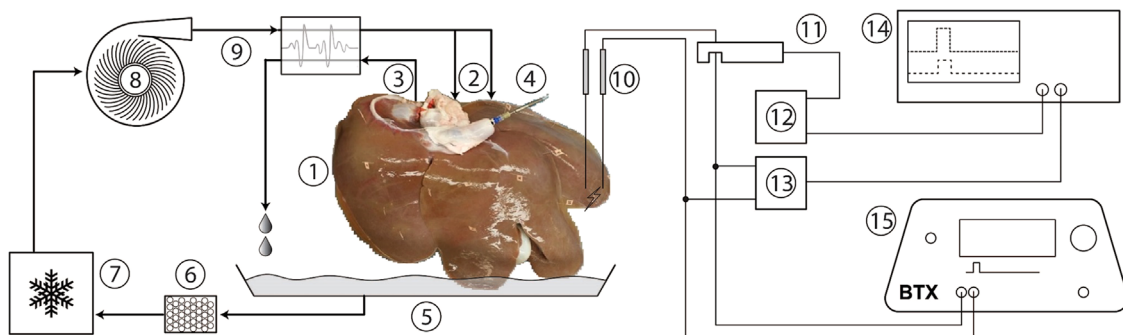

Figure 1. Schematic diagram of the perfusion and the pulse delivery system: (*1*) perfused porcine liver; (*2*) hepatic artery and portal vein as inlet; (*3*) vena cava as outlet; (*4*) temperature probe; (*5*) container; (*6*) filter; (*7*) cooler; (*8*) pump; (*9*) waveform generator; (*10*) IRE probe; (*11*) current probe; (*12*) signal conditioner; (*13*) high-voltage attenuator; (*14*) oscilloscope; (*15*) IRE pulse generator. Overall, items 1–10 are integrated into the VASOWAVE system, and items 11–14 are used for assessing electric output parameters, which are not critical to the success of the treatment.
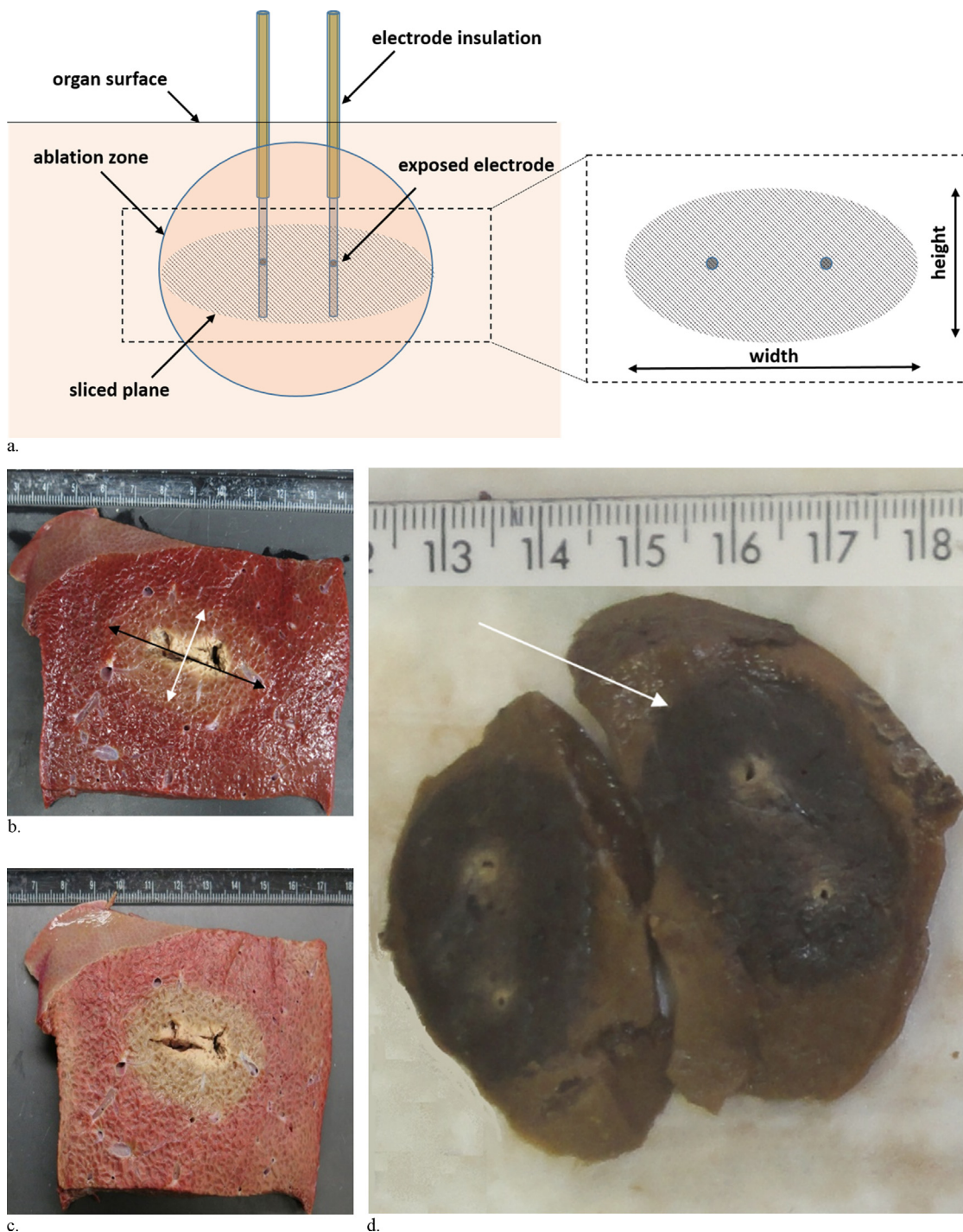
Figure 2. **(a)** Schematic showing placement of the monopolar electrodes. The sliced plane was the largest section in the middle of the IRE ablation (ie, 15 mm for parameter sets 1–5 and 10 mm for parameter sets 6–11 from surface). Diagram also shows the orientation of the width and height measured of the ablation. Ablation zone in perfused organ model obtained using parameter set 13 (2,625 V, 600 pulses, 1-cm exposure, 1.5-cm electrode spacing) **(b)** after staining with TTC and **(c)** after fixation of the stained sample in formalin for 24 hours. The ablation width and height are shown by black and white arrows, respectively. Small thermally affected zones within the greater IRE region are observable in close proximity to the probes. **(d)** Ablation zone in canine liver obtained using parameter set 10 (2,625 V, 200 pulses, 1-cm exposure, 1.5-cm electrode spacing). Arrow indicates ablation margin. Small thermally affected zones within the greater IRE region are observable in close proximity to the probes. The smaller region of thermal damage in the in vivo model compared with the perfused organ model for these images is likely due to the lower number of pulses (200 compared with 600).

condemned male greyhounds (≈ 30 kg) were procured from approved sources and acclimated ≥ 24 hours before procedures to ensure health. Trials were performed on anesthetized animals receiving pancuronium muscle blockade (**Appendix A** [available online at *www.jvir.org*]) using a similar setup to that previously described (9) and

the pulse generator and current measurement device used for the perfused organ model. Pairs of 2 19-gauge needle electrodes (1.0 mm diameter, 1.0-cm exposure) were inserted into the surgically exposed liver separated either 1.5 or 2.0 cm (center-to-center). A series of 100-μsec pulses were delivered at a pulse rate of 1/s, reversing polarity after every 50 pulses. A 5-second pause after pulses 10 and 50 enabled storing the data. The average current recorded over the last 40 μsec of the last pulse delivered was compared with the perfused organ model. There were 17 ablations performed, investigating varying electrode separation, applied voltage, and number of pulses (**Table 1**).

Determination of Treatment Effect in Canine Model. Animals were maintained under anesthesia 6 hours following electric pulse delivery before death induced by pentobarbital overdose. Livers were removed, and trial sections were separated and preserved in 10% buffered formalin for 48 hours before being sectioned into 5-mm slices and photographed. Images were blinded and analyzed with ImageJ (National Institutes of Health, Bethesda, Maryland) to determine maximum ablation width and height dimensions.

Data Analysis

Independent *t* tests were performed on individual ablation measurement widths and heights to determine statistical significance of differences between the perfused organ model and in vivo studies for each parameter setting. In addition, correlative and linear analysis was performed on comparisons between in vivo and perfused organ model ablation sizes for width and height measurements. A 95% confidence interval was plotted along the regression line.

Higher order regression analysis was conducted for comparable perfused organ model and in vivo canine data on the relationship between the number of pulses and ablation growth. One-way analysis of variance was used to analyze the effects of increasing voltages and number of pulses on ablation sizes. Additionally, independent *t* tests were performed on the final currents from the perfused organ and in vivo canine experiments. Generally, a difference with $P \leq .050$ was considered statistically significant. However, for multiple comparisons, the Bonferroni correction was applied given as .05/ number of comparisons, reducing the threshold of equivalence to $P \leq .0045$ for ablation measurements and $P \leq .0083$ for current measurements to establish statistical difference. The *t* tests and analysis of variance were performed with JMP statistical software (SAS Institute Inc, Cary, North Carolina). Regression analysis and confidence interval were calculated and plotted in Microsoft Excel 2013 (Microsoft Corporation, Redmond, Washington).

RESULTS

Ablation Zones in Perfused Organ Model and Canine Model

All trials in the perfused organ model resulted in visible ablations observable as a pale discoloration in the IRE-treated areas, which was confirmed as nonviable with TTC staining (28). Although the ablation zone was detectable visually without staining, TTC staining enhanced the contrast between the ablated and nonablated areas (**Fig 2b, c**). For in vivo treatments, the ablation zones could be visualized immediately after slicing as a dark discoloration secondary to erythrocyte extravasation inside the ablation (**Fig 2d**) (29).

Comparison of Individual In Vivo and Perfused Organ Model Ablation Dimensions

Table 2 presents the ablation dimensions measured from the perfused organ model, in vivo canine, and in vivo porcine data (20), including results of independent *t* tests (assuming equal variance) conducted between individual perfused organ model and in vivo dimensions for 11 parameter sets. Of the 22 comparisons made between the individual widths and heights of the perfused organ model and in vivo data, only 1 comparison (4.5%) showed statistical differences—parameter set 7 widths ($P = .0005$).

Linear Regression Analysis for Perfused Organ Model versus In Vivo Models

Regression analysis of the perfused organ model versus all in vivo (ie, canine and porcine) data produced correlation coefficients of $R^2 = 0.7903$ and $R^2 = 0.6957$ for ablation height and width, respectively (**Fig 3a**), and a combined correlation coefficient of $R^2 = 0.9098$ when widths and heights were analyzed together (**Fig 3b**). The 95% confidence interval along the slope of this regression line was determined as ≤ 2.2 mm. Regression analysis for the perfused organ model data compared separately with the in vivo canine data produced correlation coefficients between $R^2 = 0.9164$ and $R^2 = 0.7035$ for ablation heights and widths, respectively, and $R^2 = 0.9198$ when widths and heights were analyzed together (**Fig E2a, b** [available online at *www.jvir.org*]). Similarly, regression analysis for the perfused organ model data compared separately with the in vivo porcine data produced correlation coefficients between $R^2 = 0.6045$ and $R^2 = 0.3826$ for ablation heights and widths, respectively, and $R^2 = 0.87$ when widths and heights were analyzed together (**Fig E3a, b** [available online at *www.jvir.org*]). The linear equations of the 3 regression analyses (together, canine, porcine) are $y = 1.162x - 0.4766$, $y = 1.2143x - 0.647$, and $y = 1.0929x - 0.283$.

Table 2. Comparison of Ablation Sizes for In Vivo and Perfused Organ Model for Different Parameter Sets

Parameter Set	In Vivo Model	Ablation Width (cm)		Independent t Test	Ablation Height (cm)		Independent t Test
		In Vivo	Perfused Organ Model	P Value	In Vivo	Perfused Organ Model	P Value
1	Porcine (30)	3.11 ± 0.369	3.37 ± 0.11	.2778	2 ± 0.25	2.43 ± 0.21	.1395
2		3.0 ± 0.316	3.0 ± 0.14	1.0000	1.65 ± 0.25	2.1 ± 0.08	.0145
3		2.8 ± 0.347	2.55 ± 0.17	.2497	1.55 ± 0.30	1.72 ± 0.05	.1968
4		3.24 ± 0.568	2.95 ± 0.17	.3630	1.6 ± 0.10	1.7 ± 0.08	.2275
5		3.16 ± 0.23	2.95 ± 0.23	.2221	1.7 ± 0.20	1.65 ± 0.21	.4881
6	Canine	3.01 ± 0.174	3.2 ± 0.30	.3936	1.53 ± 0.211	1.67 ± 0.06	.3247
7		4.61 ± 0.139	3.71 ± 0.28	.0005*	2.34 ± 0.213	2.39 ± 0.32	.6015
8		2.88 ± 0.169	3.2 ± 0.26	.1537	1.64 ± 0.069	2.07 ± 0.25	.0473
9		3.37 ± 0.537	3.35 ± 0.23	.8933	1.97 ± 0.120	2.14 ± 0.17	.1182
10		4.03 ± 0.316	3.96 ± 0.11	.7510	2.52 ± 0.214	2.6 ± 0.1	.5270
11		4.22 ± 0.434	4.11 ± 0.38	.7332	2.66 ± 0.214	2.62 ± 0.11	.7425
12	NA		3.91 ± 0.28			2.52 ± 0.09	
13			4.28 ± 0.36			3.12 ± 0.38	
14			3.80 ± 0.1			2.33 ± 0.15	

NA = not available.

*Indicates statistical significance based on required $P < .0045$ as obtained from the Bonferroni correction.
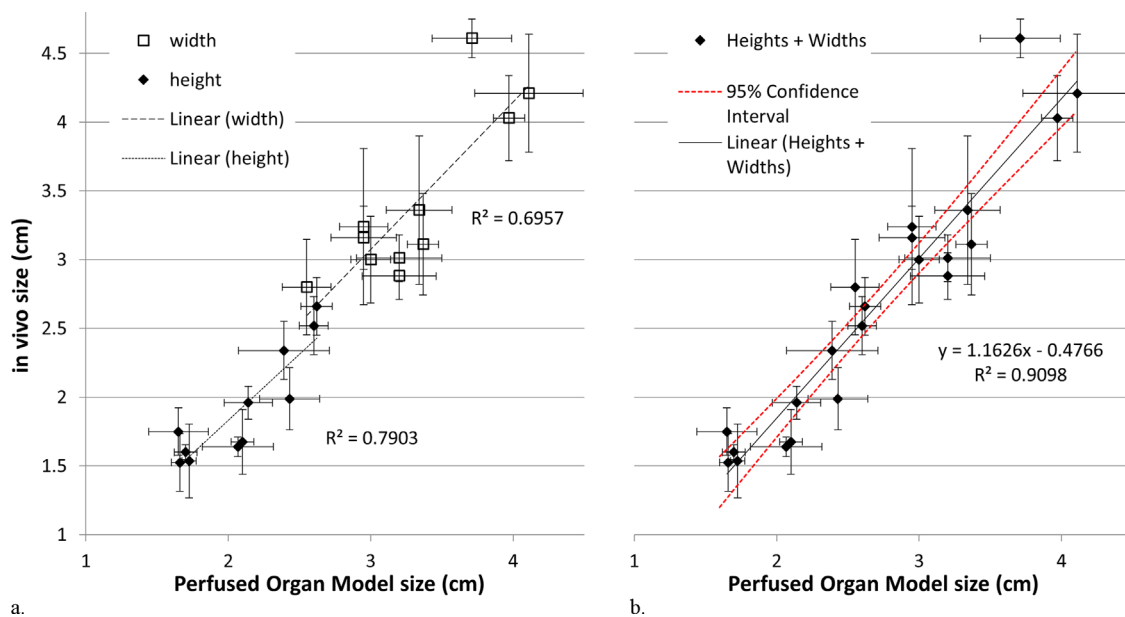

Figure 3. Linear correlation of ablation **(a)** width and height considered separately and **(b)** together for perfused organ model versus all in vivo models.

Effect of Increasing IRE Pulses and Voltages

The in vivo experiments performed on canine liver demonstrated that increasing pulse number from 50 to 200 yielded statistically significant increases in ablation ($P = .0016$ width, $P = .0007$ height). However, no significant growth was observed when increasing the number of pulses from 200 to 400 ($P = .5871$ width, $P = .4333$ height). The perfused organ followed the same trend as the canine livers, with statistically significant increases for increasing pulse numbers from 50 to 200 ($P = .0005$ width, $P = .0011$ height) and increases in pulse numbers from 200 to 400 without significance ($P = .5665$ width, $P = .8056$ height). Thus, the validated perfused model showed that the IRE ablation zone grows logarithmically with increasing pulse numbers, with minimal difference in ablation size from 200 to 600 pulses (3.2 mm ± 3.8 width, 5.2 mm ± 3.9 height). By fitting the data for width and height of the ablations in the perfused organ model to separate logarithmic
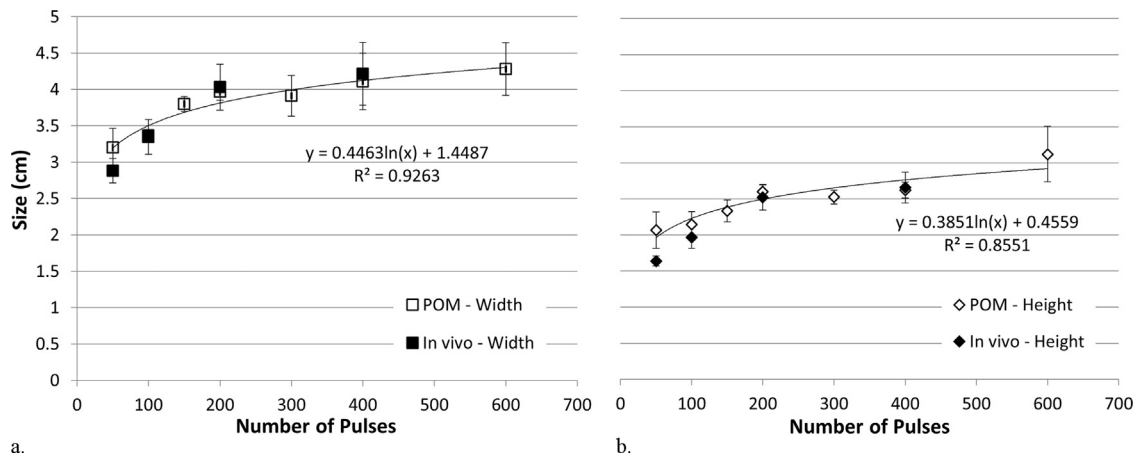
Figure 4. Growth of ablation size **(a)** width and **(b)** height by increasing the number of pulses (treatment parameter sets 8–13). The curves represent the logarithmic fit to the dimensions obtained in the perfused organ model (POM).

functions (**Fig 4a, b**), the following relations were obtained as a function of pulse number, N:

Width: $W = 0.446 \ln(N) + 1.448 \; (\text{R}^2 = 0.9263)$

Height: $H = 0.385 \ln(N) + 0.455 \; (\text{R}^2 = 0.8551)$

Furthermore, the treatment effect in the perfused organ model was similar to prior in vivo porcine models. Changing the parameters such as voltage and pulse numbers had similar effects on the ablation size for the perfused organ model and in vivo models (**Fig 5a–d**). Perfused organ ablations showed a statistically significant increase in widths and heights when the applied voltage increased from 2,250 to 3,000 V ($P = .0003$ width, $P = .0002$ height) (**Fig 5a, b**). The perfused organ also emulated the response of the in vivo porcine livers to increasing pulses (**Fig 5c, d**).

Electric Current Measurements

Overall, it was found that the currents recorded at the end of the treatments for the perfused organ model were higher than those recorded for the canine experiments (**Table E1** [available online at *www.jvir.org*]). However, only 1 of 6 comparisons (parameter set 9) showed statistical difference between the in vivo and canine experiments. For most treatments, the current recorded was higher when the number of pulses was increased or when the applied voltage was increased.

DISCUSSION

In this study, the feasibility of using a perfused organ model as a platform to study the IRE outcome under varying treatment parameters was investigated. Live animal models are costly and logistically complex because of the need to maintain the animals as well as a full operating theater to maintain a vital animal during the pulse protocol. Use of the perfused organ model for this application provides a potentially more accessible platform for a multitude of additional preclinical experiments to characterize and optimize IRE outcomes for future enhancements of this therapy. This study demonstrated a strong correlation overall ($R^2 = 0.9098$) between ablations obtained in the perfused organ model versus in vivo ablations, validating the perfused organ model for IRE therapy outcome characterization under varying conditions. Performing IRE treatments on an explanted porcine liver undergoing active perfusion has been reported before (24). However, that study was proposed primarily to develop decellularized tissue scaffolds, without comparing the IRE outcomes against in vivo data.

This study demonstrates the feasibility of using a perfused organ model for studying effects of pulse parameters and electrode configurations on IRE ablation zones Specifically, it has been shown that, for a given set of pulse parameters and electrode configurations (spacing, exposure, and pulse number), the perfused organ model and in vivo livers have statistically equivalent ablation sizes for almost all treatment parameter sets, with a single difference potentially attributed to the low sample size of the in vivo data. For in vivo treatments, the ablation zones could be visualized immediately after slicing as a dark discoloration resulting from erythrocyte extravasation inside the ablation (29). However, this is not the case for perfused organ model ablations because removal of all the blood from the vasculature eliminated discoloring erythrocyte extravasation.

The overall regression analysis reveals a tight correlation between the obtained in vivo ablation sizes and ablation sizes in the perfused organ model. However, the slight deviations of the slope and intercept of the regression line from the ideal case of $y = x$ indicates that the perfused organ model and in vivo models show some differences in response to IRE. Several experimental conditions might be responsible for this difference. Pausing the perfusion during the treatment could
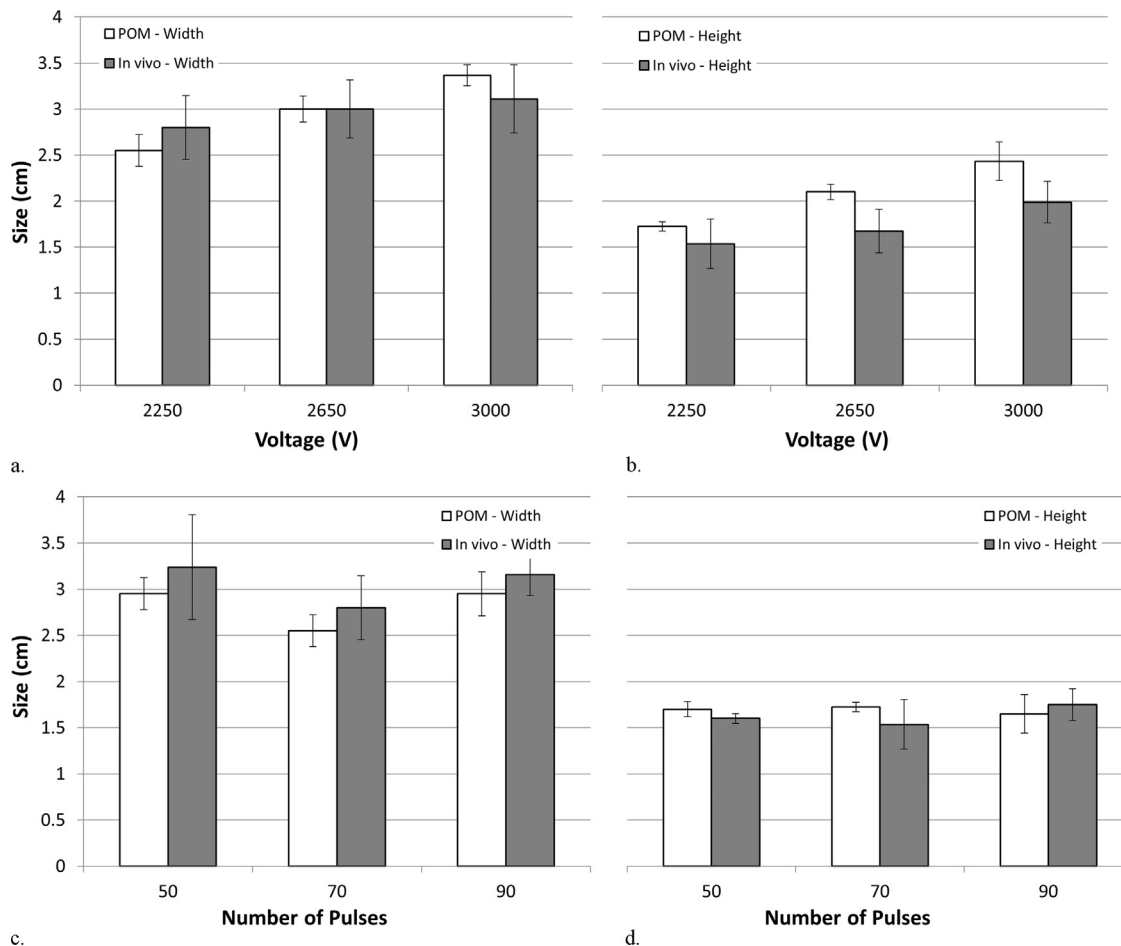
Figure 5. Comparison of ablation dimensions **(a)** width and **(b)** height, parameter set 1 (3,000 V, 2-cm exposure, 1.5-cm spacing, 70 pulses), parameter set 2 (2,650 V, 2-cm exposure, 1.5-cm spacing, 70 pulses), and parameter set 3 (2,250 V, 2-cm exposure, 1.5-cm spacing, 70 pulses). Comparison of ablation dimensions **(c)** width and **(d)** height for different number of pulses between porcine liver and perfused organ model (POM), parameter set 3 (2,250 V, 2-cm exposure, 1.5-cm spacing, 70 pulses), parameter set 4 (2,250 V, 2-cm exposure, 1.5-cm spacing, 50 pulses), and parameter set 5 (2,250 V, 2-cm exposure, 1.5-cm spacing, 90 pulses).

potentially cause the liver to contract, and owing to the smaller volume of the liver, more cells are exposed to the electroporation-inducing electric fields, causing a larger ablation. Other factors, such as higher electric conductivity and lower temperature of the perfusate, might also influence the ablation size and cause differences between the models. Consistent with the higher perfusate conductivity, the currents recorded at the end of treatment are higher in the perfused organ model than in the in vivo canine experiments and are representative of the differences between the models. However, these currents for most parameter sets are not statistically different. Likewise, the linear regression analyses of the in vivo canine model versus perfused organ model and in vivo porcine model versus perfused organ model conducted separately show different correlation coefficients, slopes, and intercepts. These differences could be attributed to differences in the pulse repetition rate between the porcine and canine data and/or tissue-to-tissue and species-to-species variability. Regardless, future studies are needed to quantitatively investigate these factors.

Apart from its validation, the perfused organ model was used to study the effect of increasing pulse numbers on the ablation dimensions. Finding the optimum number of pulses for treatments is of critical importance in terms of maximizing ablation size, while minimizing treatment time and avoiding thermal damage to the tissue. It was shown here that when the pulse numbers are increased from 50 to 600 with the fixed amplitude of 2,625 V, the ablation sizes follow a logarithmically increasing trend, indicating that increasing pulse numbers beyond 200 has little additional effect on the ablation sizes. This logarithmic response of cells to electroporation-inducing fields has been observed in previous in vitro studies (30). However, the present study validates this trend beyond the 128 IRE pulses previously reported.

As a validated platform, the perfused organ model could be used widely to further enhance the field of electroporation-based therapies. This includes investigating different pulse timing algorithms, electric current and arcing conditions, ablation size lookup tables (sets of

separation and voltage), and new device development and optimization. Although the feasibility of this model was shown in the liver, other organs such as the kidney and pancreas could also be tested. The liver was chosen for this study because the greatest collections of preclinical and clinical investigations of IRE exist for the liver (22,31). This might be because, as opposed to other thermal-based therapies, IRE has shown preservation of structures surrounding liver tumors, including bile ducts, bowel, and gallbladder (32).

Future studies may investigate simpler perfusion systems or circuits. Although the active perfusion system here used a cardioemulating pulse with several additional features to mimic physiologic conditions and maintain viability, it does not preclude the ability to perform perfused organ model trials with other modalities for attaining active perfusion. For instance, although the most representative system was used to prove out the feasibility of a validated model, a basic peristaltic pump perfusion system with a well-developed perfusate optimized to maintain tissue viability may also prove sufficient for attaining viable preclinical trial data.

This study has some limitations that are expected to be addressed in future works. Similar to prior IRE in vivo studies, this study was performed only on livers, and the response needs to be verified for other organs. The livers in this study were healthy and did not have any tumors. Also, the fact that perfusion was stopped during the treatment may cause minor alterations to the ablation outcome as noted earlier.

In conclusion, this study tested the validity of a novel perfused organ model for evaluating ablation zone characteristics from IRE therapies under varying conditions. The ablation zone outcomes from the perfused organ model were validated against data from in vivo studies and found to be statistically equivalent to in vivo ablation outcomes. This model may hold promise for expediently determining the outcomes from manipulating further complex aspects of IRE therapy delivery, such as the introduction of delays between sets of pulses or introducing environment-altering agents to enable more optimal and efficient IRE application in clinical practice.

ACKNOWLEDGMENTS

REFERENCES

1. Davalos RV, Mir IL, Rubinsky B. Tissue ablation with irreversible electroporation. Ann Biomed Eng 2005; 33:223–231.
2. Al-Sakere B, Andre F, Bernat C, et al. Tumor ablation with irreversible electroporation. PLoS One 2007; 2:e1135.
3. Weaver JC. Electroporation: a general phenomenon for manipulating cells and tissues. J Cell Biochem 1993; 51:426–435.
4. Lee RC, Canaday DJ, Hammer SM. Transient and stable ionic permeabilization of isolated skeletal muscle cells after electrical shock. J Burn Care Rehabil 1993; 14:528–540.
5. Rubinsky B. Irreversible electroporation in medicine. Technol Cancer Res Treat 2007; 6:255–260.
6. Neal RE 2nd, Millar JL, Kavnoudias H, et al. In vivo characterization and numerical simulation of prostate properties for non-thermal irreversible electroporation ablation. Prostate 2014; 74:458–468.
7. Wimmer T, Srimathveeravalli G, Gutta N, et al. Comparison of simulation-based treatment planning with imaging and pathology outcomes for percutaneous CT-guided irreversible electroporation of the porcine pancreas: a pilot study. J Vasc Interv Radiol 2013; 24:1709–1718.
8. Corovic S, Lackovic I, Sustaric P, et al. Modeling of electric field distribution in tissues during electroporation. Biomed Eng Online 2013; 12:16.
9. Neal RE 2nd, Garcia P, Kavnoudias H, et al. In vivo irreversible electroporation kidney ablation: experimentally correlated numerical models. IEEE Trans Biomed Eng 2015; 62:561–569.
10. Pucihar G, Kotnik T, Miklavčič D, et al. Kinetics of transmembrane transport of small molecules into electropermeabilized cells. Biophys J 2008; 95:2837–2848.
11. Yarmush M, Golberg A, Serša G, Kotnik T, Miklavčič D. Electroporation-based technologies for medicine: principles, applications, and challenges. Annu Rev Biomed Eng 2014; 16:295–320.
12. Arena CB, Szot CS, Garcia PA, Rylander MN, Davalos RV. A three-dimensional in vitro tumor platform for modeling therapeutic irreversible electroporation. Biophys J 2012; 103:2033–2042.
13. Sano MB, Arena CB, Bittleman KR, et al. Bursts of bipolar microsecond pulses inhibit tumor growth. Sci Rep 2015; 5:14999.
14. Martin RC, McFarland K, Ellis S, Velanovich V. Irreversible electroporation therapy in the management of locally advanced pancreatic adenocarcinoma. J Am Coll Surg 2012; 215:361–369.
15. Thomson KR, Cheung W, Ellis SJ, et al. Investigation of the safety of irreversible electroporation in humans. J Vasc Interv Radiol 2011; 22:611–621.
16. Kingham TP, Karkar AM, D'Angelica MI, et al. Ablation of perivascular hepatic malignant tumors with irreversible electroporation. J Am Coll Surg 2012; 215:379–387.
17. Bitsch RG, Düx M, Helmberger T, Lubienski A. Effects of vascular perfusion on coagulation size in radiofrequency ablation of ex vivo perfused bovine livers. Invest Radiol 2006; 41:422–427.
18. Arefiev A, Prat F, Chapelon JY, Tavakkoli J, Cathignol D. Ultrasound-induced tissue ablation: studies on isolated, perfused porcine liver. Ultrasound Med Biol 1998; 24:1033–1043.
19. Dodd GD III, Dodd NA, Lanctot AC, Glueck DA. Effect of variation of portal venous blood flow on radiofrequency and microwave ablations in a blood-perfused bovine liver model. Radiology 2013; 267:129–136.
20. Ben-David E, Appelbaum L, Sosna J, Nissenbaum I, Goldberg SN. Characterization of irreversible electroporation ablation in in vivo porcine liver. AJR Am J Roentgenol 2012; 198:W62–W68.
21. Appelbaum L, Ben-David E, Faroja M, Nissenbaum Y, Sosna J, Goldberg SN. Irreversible electroporation ablation: creation of large-volume ablation zones in in vivo porcine liver with four-electrode arrays. Radiology 2014; 270:416–424.
22. Scheffer HJ, Nielsen K, de Jong MC, et al. Irreversible electroporation for nonthermal tumor ablation in the clinical setting. J Vasc Interv Radiol 2014; 25:997–1011; quiz 1011.
23. Zu TNK, Athamneh AIM, Collakova E, et al. Assessment of ex vivo perfused liver health by raman spectroscopy. J Raman Spectrosc 2015; 46:551–558.
24. Sano MB, Neal RE, Garcia PA, Gerber D, Robertson J, Davalos RV. Towards the creation of decellularized organ constructs using irreversible electroporation and active mechanical perfusion. Biomed Eng Online 2010; 9:83.
25. Duck FA. Physical Properties of Tissues: A Comprehensive Reference Book. London: Academic Press; 2013.
26. Edd JF, Horowitz L, Davalos RV, Mir LM, Rubinsky B. In vivo results of a new focal tissue ablation technique: irreversible electroporation. IEEE Trans Biomed Eng 2006; 53:1409–1415.
27. Lee EW, Chen C, Prieto VE, Dry SM, Loh CT, Kee ST. Advanced hepatic ablation technique for creating complete cell death: irreversible electroporation. Radiology 2010; 255:426–433.
28. Charpentier KP, Wolf F, Noble L, Winn B, Resnick M, Dupuy DE. Irreversible electroporation of the liver and liver hilum in swine. HPB (Oxford) 2011; 13:168–173.

29. Appelbaum L, Ben-David E, Sosna J, Nissenbaum Y, Goldberg SN. US findings after irreversible electroporation ablation: radiologic-pathologic correlation. Radiology 2012; 262:117–125.

30. Pucihar G, Krmelj J, Reberšek M, Napotnik TB, Miklavčič D. Equivalent pulse parameters for electroporation. IEEE Trans Biomed Eng 2011; 58:3279–3288.

31. Charpentier KP. Irreversible electroporation for the ablation of liver tumors: are we there yet? Arch Surg 2012; 147:1053–1061.

32. Cannon R, Ellis S, Hayes D, Narayanan G, Martin RC 2nd. Safety and early efficacy of irreversible electroporation for hepatic tumors in proximity to vital structures. J Surg Oncol 2013; 107:544–549.

APPENDIX A.
SUPPLEMENTAL MATERIALS AND METHODS

Composition of Modified Phosphate-Buffered Saline Solution

The modified phosphate-buffered saline solution for perfusion of the liver model contained sodium chloride (NaCl; 137 mmol/L), potassium chloride (KCl; 2.7 mmol/L), disodium phosphate (Na_2HPO_4; 10 mmol/L), monopotassium phosphate (KH_2PO_4, 1.8 mmol/L), calcium chloride ($CaCl_2$, 1 mmol/L), and magnesium chloride ($MgCl_2$, 0.5 mmol/L).

Perfusion Model Electric Measurement Equipment

For the perfusion model, an oscilloscope (DPO2002B; Tektronix, Inc, Beaverton, Oregon) was used to view the output waveforms using a 50-MHz 1,000× high-voltage probe (P5210A; Tektronix, Inc), and the current was measured using an active clamp on a 50-MHz current probe (TCP305; Tektronix, Inc) (Fig 1).

In Vivo Canine Model Electric Measurement Equipment

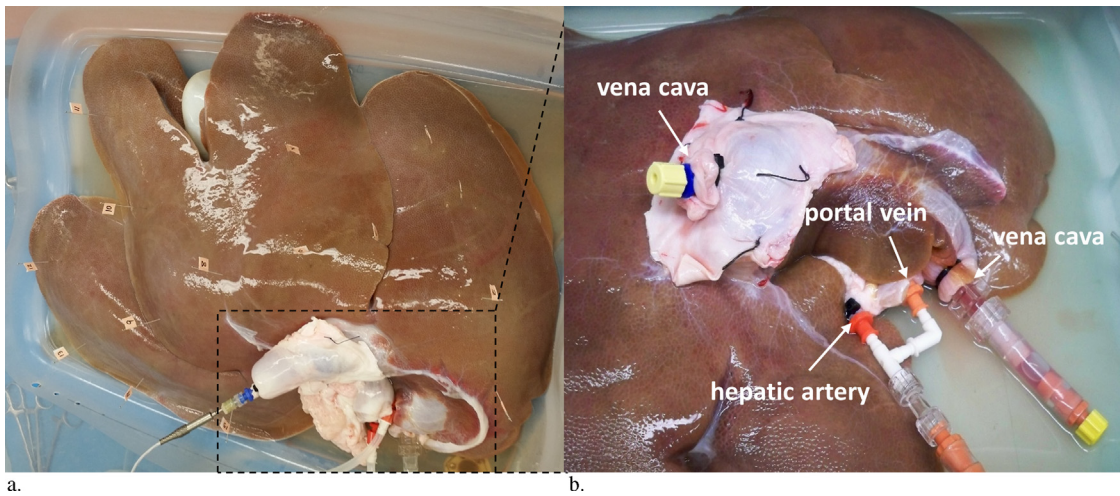For the canine model, a Protek DSO-2090 USB computer-interface oscilloscope (GS Instruments Co,

Figure E1. **(a)** Porcine liver being perfused on VASOWAVE perfusion system. **(b)** Connections made to the excised liver: portal vein, hepatic artery, and vena cava.
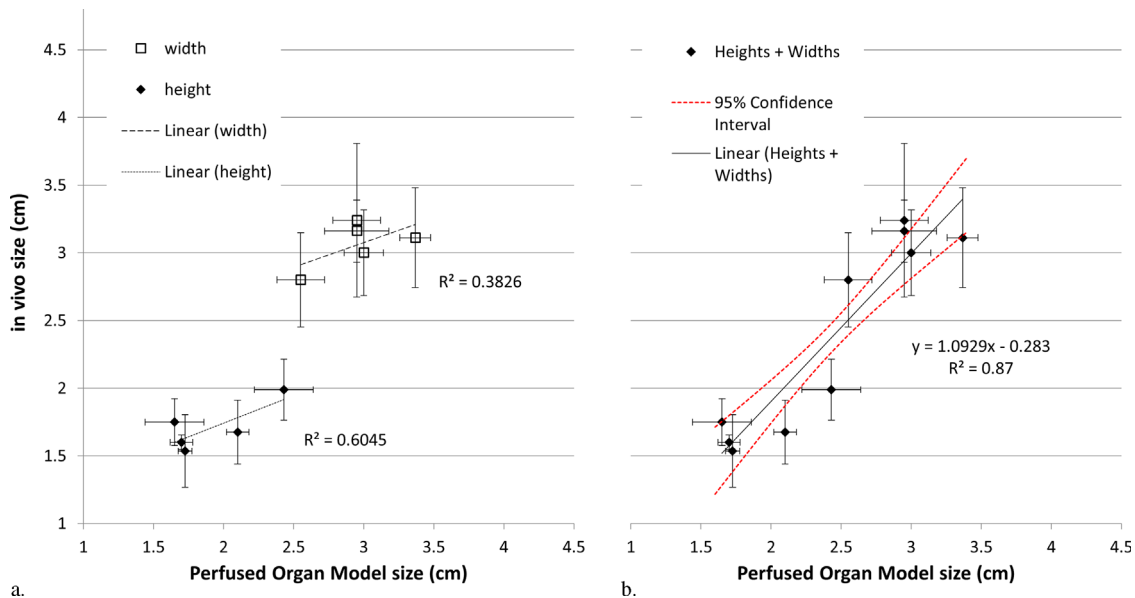

Figure E2. **(a, b)** Linear correlation of ablation dimensions for in vivo canine versus perfused organ model.

Ltd, Incheon, Korea) provided current measurements on a laptop using DSO-2090 software (GS Instruments Co, Ltd).

Experimental Procedure on Canine Model

Before the procedure, subjects were administered acepromazine (0.1 mg/kg), atropine (0.05 mg/kg), and morphine (0.2 mg/kg), and then general anesthesia was induced with propofol (6 mg/kg, then 0.5 mg/kg/min) and maintained with inhaled isoflurane (1%–2%). After ensuring adequate anesthesia (monitored with electroencephalography brain activity bispectral index), a midline incision was made, and tissues were maneuvered to access the liver. Immediately before pulse delivery, pancuronium was delivered intravenously to mitigate electrically mediated muscle contraction (initial 0.2 mg/kg dose, adjusted to contraction intensity).
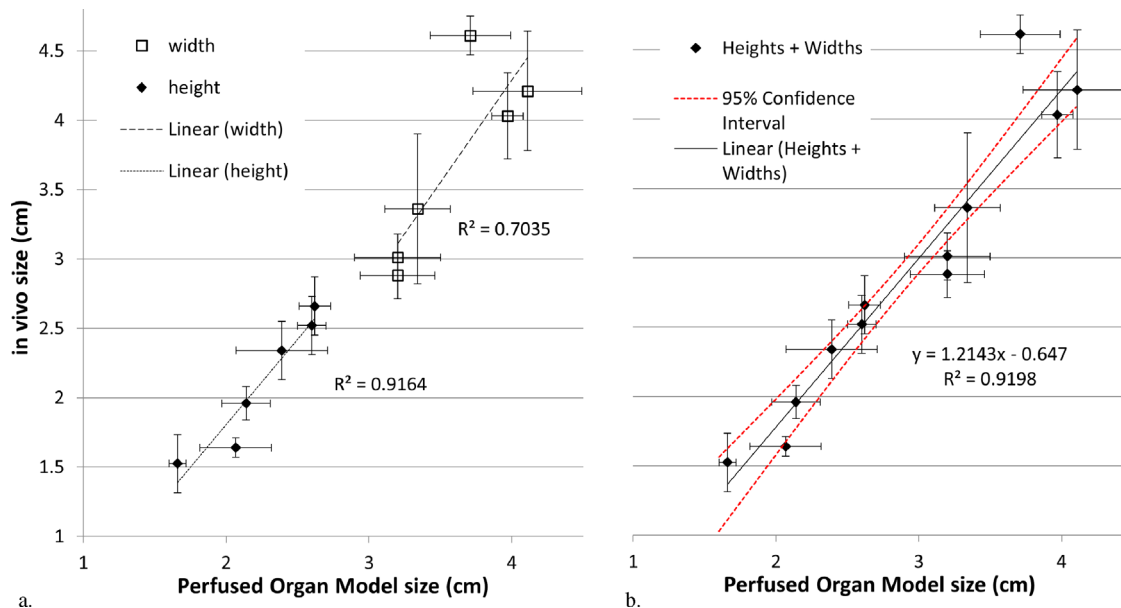

Figure E3. **(a, b)** Linear correlation of ablation dimensions for in vivo porcine versus perfused organ model.

Table E1. Electric Currents at the End of Treatment for Perfused Organ and In Vivo (Canine) Model

	Current Recorded at End of Treatment (A)		Independent *t* Test
Parameter Set	In Vivo (Canine)	Perfused Organ Model	P Value
1		56 ± 13.06	
2		31.23 ± 5.74	
3		26.2 ± 2.64	
4		18.9 ± 1.05	
5		20.7 ± 5.02	
6	6.74 ± 1.08	14 ± 5.29	.166
7	23.2 ± 13.4	23.73 ± 4	.8563
8	29.11 ± 15.89	30.13 ± 12.93	.9413
9	15.5 ± 4	23.41 ± 4.11	.0016*
10	14 ± 0.94	22.66 ± 3.06	.0093
11	28.09 ± 0.4	34.2 ± 15.37	.6177
12		24.5 ± 3.7	
13		28.83 ± 6.74	
14		15 ± 2.65	

*Indicates statistical significance based on the required $P < .0083$ as obtained from the Bonferroni correction.